Geophys. J. Int. (1997) **129**, 450–460

Fully normalized spherical cap harmonics: application to the analysis of sea-level data from TOPEX/POSEIDON and ERS-1

Cheinway Hwang and Shin-Kuen Chen

Department of Civil Engineering, National Chiao Tung University, 1001 *Ta Hsueh Road, Hsinchu* 30050, *Taiwan. E-mail: hwang@geodesy.cv.nctu.edu.tw*

Accepted 1997 January 21. Received 1997 January 10; in original form 1996 July 24

SUMMARY

We introduce two sets of fully normalized harmonics for the spectral analysis of functions defined on a spherical cap. The harmonics are the products of Fourier functions and the fully normalized associated Legendre functions of non-integer degree. Using Sturm–Liouville theory for boundary-value problems, we present two convenient and stable formulae for computing the zeros of the associated Legendre functions that form two sets of orthogonal functions. Formulae for the stable numerical evaluation of the fully normalized associated Legendre functions of non-integer degree that avoid the gamma function are also derived. The result from the expansions of sea-level anomaly from altimetry into Set 2 fully normalized cap harmonics shows fast convergence of the series, and the degree variances decay rapidly without aliasing effects. The zero-degree coefficients (Set 2) of sea-level anomaly from TOPEX/POSEIDON (T/P) and ERS-1 indicate an El Niño event during 1993 January–1993 July, and a La Niña event during 1993 November–1994 July, although the ERS-1 result is less obvious. Ocean circulations over the South China Sea and the Kuroshio area are clearly identified with the low-degree expansions of sea-surface topography (SST) from T/P and ERS-1. A cold-core eddy of 4° in diameter centred at 17.5°N, 118°E was detected with the expansion of SST from T/P cycle 47, and a property of the cap harmonics is used to compute this eddy's kinetic energy. The kinetic energy is at a low in winter and high in summer, and its variation seems to be periodic with an amplitude of 0.4 $m^2 s^{-2}$.

Key words: satellite geodesy, sea-level, spectral analysis, spherical harmonics.

1 INTRODUCTION

The almost complete treatment of Legendre functions of general type by Hobson (1965) includes the topic of associated Legendre functions of non-integer degree. However, it was Haines (1985a,b) who first made use of these functions in approximating the geomagnetic field with the introduction of spherical cap harmonics. Other applications of spherical cap harmonics are mostly found in geomagnetic literature; for example in De Santis (1991) and Haines & Torta (1994). A simple approximated alternative based on ordinary spherical harmonics properly adjusted to the cap is given by De Santis (1992). In the geodetic literature, applications have been found in, for example, Hwang (1991), who clarified the relationship between the associated Legendre function and the hypergeometric function, and Li, Chao & Ning (1995), who employed spherical cap harmonic expansions for the gravity field representation over China. In fact, the associated Legendre function used by Haines (1985a) was based on Schmidt normalization, and he used certain approximations in the normalizing factor which presumably did not affect his results. This paper will review the theory of associated Legendre function of general type by the eigenfunction–eigenvalue approach and introduce two sets of fully normalized spherical cap harmonics. The term 'fully' is used by analogy with the fully normalized spherical harmonics (Heiskanen & Moritz 1967), which offer convenient computational formulae and have many advantages in interpreting the spectral components of a function defined on a cap. Also, new and rigorous formulae will be derived, as compared to the formulae used in, for example, Haines (1988) and De Santis (1991, 1992). The motivation of this study is to find basis functions other than ordinary spherical harmonics that can be used to represent local sea-level data derived from satellite altimetry. After introducing the fully normalized spherical cap harmonics, we will use the harmonic expansions to study the oceanographic signals obtained with the TOPEX/POSEIDON (T/P) and ERS-1 missions.

2 THEORY OF FULLY NORMALIZED SPHERICAL CAP HARMONICS

2.1 Associated Legendre functions and hypergeometric functions

It is known (e.g. Hobson 1965; Lebedev 1972; Hwang 1991) that Legendre's function can be represented by the hypergeometric function which then can be used to derive a general type of Legendre function. The hypergeometric function is defined as (Lebedev 1972)

$$F(a,b;c;z)=u=\sum_{k=0}^{\infty}\frac{(a)_k(b)_k}{k!(c)_k}z^k,\quad |z|<1, \tag{1}$$

where $(a)_n$, $(b)_n$, and $(c)_n$, are shifted factorials defined as

$$(a)_0=1,\quad (a)_n=a(a+1)\ldots(a+n-1),\quad n=1,2,\ldots \tag{2}$$

By a simple change of variable in the differential equation associated with the hypergeometric function, we can obtain Legendre's differential equation, which leads to the representation of Legendre's function in terms of the hypergeometric function:

$$P_\ell(t)=F\left(-\ell,\ell+1;1;\frac{1-t}{2}\right). \tag{3}$$

When ℓ is an integer, by the definition of the shifted factorial in (2) we see that a coefficient in the series is zero if $k>\ell$. In this case, $P_\ell(t)$ is a polynomial of degree ℓ.

Furthermore, using the definition of the associated Legendre function,

$$P_\ell^m(t)=(1-t^2)^{m/2}\frac{d^m}{dt^m}(P_\ell), \tag{4}$$

and the property of the hypergeometric function that

$$\frac{d}{dz}F(a,b;c;z)=\frac{ab}{c}F(a+1,b+1;c+1;z), \tag{5}$$

the associated Legendre function can be represented in terms of the hypergeometric function:

$$\begin{aligned}P_\ell^m(t)&=\frac{(-1)^m}{2^m m!}(-\ell)_m(\ell+1)_m(1-t^2)^{m/2}\\&\quad\times F\left(m-\ell,m+\ell+1;m+1;\frac{1-t}{2}\right)\\&=\frac{1}{2^m m!}\frac{\Gamma(\ell+m+1)}{\Gamma(\ell-m+1)}(1-t^2)^{m/2}\\&\quad\times F\left(m-\ell,m+\ell+1;m+1;\frac{1-t}{2}\right),\end{aligned} \tag{6}$$

where $\Gamma(z)$ is the gamma function defined as

$$\Gamma(z)=\int_0^\infty \mathrm{e}^{-t}t^{z-1}\,dt,\quad z>0, \tag{7}$$

which has the property $\Gamma(z+1)=z\Gamma(z)$.

In (6), m must be a non-negative integer because of (4), but there is no restriction on ℓ. If ℓ is a non-negative integer, then $\Gamma(\ell+m+1)=(\ell+m)!$ and $\Gamma(\ell-m+1)=(\ell-m)!$, and, if $m>\ell$, then according to (4) $P_\ell^m(t)=0$. Also, if $\ell\geq m$, then $F(m-1,m+\ell+1;m+1;[1-t]/2)$ is a polynomial of degree $(\ell-m)$. Therefore, formula (6) is also valid for the Legendre function of the first kind described in Heiskanen & Moritz (1967, p. 22) and holds for the closed interval $[-1,1]$. If ℓ is non-integer, then P_ℓ^m can be expressed in a hypergeometric series with an infinite number of terms:

$$P_\ell^m(t)=\frac{1}{2^m m!}\frac{\Gamma(\ell+m+1)}{\Gamma(\ell-m+1)}(1-t^2)^{m/2}\sum_{k=0}^{\infty}a_k\left(\frac{1-t}{2}\right)^k, \tag{8}$$

where the coefficients a_k can be found by the recursive formula

$$a_0=1,\ a_k=\frac{(m-\ell+k-1)(m+\ell+k)}{k(m+k)}a_{k-1}. \tag{9}$$

The series in (8) converges rapidly if t is near 1, and goes to infinity if $t=-1$. To evaluate the series in (8), for given ℓ and m we can define a small positive number ε, depending on the desired accuracy, and introduce the truncated series S_N as

$$S_N=\sum_{k=0}^{N}a_k\left(\frac{1-t}{2}\right)^k. \tag{10}$$

If $|S_{N+1}-S_N|\leq\varepsilon$, then the series is truncated at N.

2.2 The zeros of $P_\ell^m(t)$ and $dP_\ell^m(t)/dt$ as functions of ℓ

When constructing orthogonal systems from the associated Legendre functions, we need to find the zeros (roots) of $P_\ell^m(t)$ and $dP_\ell^m(t)/dt$ as functions of ℓ. These zeros correspond to the eigenvalues of the solution of the Sturm–Liouville boundary-value problem (e.g. Courant & Hilbert 1953; Hwang 1991; De Santis & Falcone 1995). First, Legendre's differential equation can be expressed in Sturm–Liouville form as

$$\frac{d}{dt}\left[(1-t^2)\frac{dP_\ell^m(t)}{dt}\right]+\left[\ell(\ell+1)-\frac{m^2}{1-t^2}\right]P_\ell^m(t)=0, \tag{11}$$

subject to the boundary condition (BC) at $t=t_0$

$$AP_{\ell_k}^m(t_0)+B\frac{dP_{\ell_k}^m(t_0)}{dt}=0,\quad k=i,j, \tag{12}$$

where $\ell(\ell+1)$ is the eigenvalue of $P_\ell^m(t)$, and

$$\frac{dP_{\ell_i}^m(t_0)}{dt}=\left.\frac{dP_{\ell_i}^m(t)}{dt}\right|_{t=t_0}.$$

In (12), the cases with (1) $A\neq0, B=0$, (2) $A=0, B\neq0$ and (3) $A\neq0, B\neq0$ correspond to Dirichlet, Neumann and mixed boundary conditions, respectively. By selecting appropriate A and B we say that the BC in Case 3 is 'natural' when the set of basis functions associated with this BC are used to represent an arbitrary function over $t_0\leq t\leq 1$. Here we will only pursue the BC in cases 1 and 2. By considering $P_\ell^m(t_0)$ and $P_\ell^m(t_0)/dt$ as two functions of ℓ, and then solving separately the equations (Hwang 1991; Haines 1985a)

$$P_\ell^m(t_0)=0, \tag{13}$$

$$\frac{dP_\ell^m(t_0)}{dt}=0, \tag{14}$$

we obtain two different sets of orthogonal functions (the functions are orthogonal only within one set). For this purpose, the hypergeometric representation of $P_\ell^m(t)$ is needed. The function $dP_\ell^m(t_0)/dt$ can be obtained by the recursive formula

$$(t^2-1)\frac{dP_\ell^m(t)}{dt}=\ell tP_\ell^m(t)-(\ell+m)P_{\ell-1}^m(t) \tag{15}$$

(Lebedev 1972, p. 195), or by term-wise differentiation in the hypergeometric series of $P_\ell^m(t)$ as in Haines (1988, p. 415).

When finding the zeros, it is useful to avoid computing the gamma functions or the shifted factorials because they can be very large and can cause numerical problems. To do this, we first remove the common factors involving m and t_0 from (13) and (14) because they do not affect the result. Referring to (6), the shifted factorials $(-\ell)_m(\ell+1)_m$ are also removed from (13) and (14) because ℓ is non-integer and the zeros cannot be obtained by setting the shifted factorials equal to zero. By such a manipulation, we obtain simplified equations from (13) and (14):

$$F(\ell, m, t_0) = 0 \tag{16}$$

$$\ell t_0 F(\ell, m, t_0) - (\ell - m)F(\ell - 1, m, t_0) = 0, \tag{17}$$

where

$$F(\ell, m, t) = F\left(m - \ell, m + \ell + 1; m + 1; \frac{1-t}{2}\right)$$

is the simplified notation for the hypergeometric function. There is no numerical problem in using (16) and (17) for finding the zeros. The methods of computing zeros based on (16) and (17) are to be compared with those of Haines (1988).

2.3 The index of zero and frequency classification of $P_\ell^m(t)$

The eigenfunctions such as $P_\ell^m(t)$ derived from a Sturm–Liouville problem form a complete set of functions which can be used for the spectral decomposition of a function. For a given t_0 and m we will obtain an infinite number of zeros by solving (16) or (17), each associated with an eigenvalue and an eigenfunction. We denote these zeros by ℓ_n, $n = 1, 2, \ldots$, and $\ell_{n+1} > \ell_n$. The value ℓ_n will be called the 'degree at index n'. Now, a theorem of Courant & Hilbert (1953, p. 454) states that, 'the nth eigenfunction for a Sturm–Liouville problem divides the fundamental domain into precisely n parts by means of its nodal points'. Thus, by this theorem $P_{\ell_{n+1}}^m$ will change its sign once more than $P_{\ell_n}^m$ over $t_0 \le t \le 1$. Also, it is known (Hobson 1965, p. 386) that $P_\ell^m(t)$ as a function of t has no zero if $m \ge \ell$. Based on these observations, and in order to have the same frequency classification as the associated Legendre function of integral degree (see Heiskanen & Moritz 1967, p. 25), for a given m we denote the first zero from the solution of (16) or (17) by ℓ_m so that the function $P_{\ell_n}^m$ changes its sign $(n-m)$ times over $t_0 \le t \le 1$. (It can be shown that the first zero ℓ_m is greater than or equal to m.) Table 1 lists the zeros up to $n = m = 8$ for $\theta_0 = 10°$ that will be used below. Fig. 1 shows the associated Legendre functions of non-integer degree for $\theta_0 = 10°$ and $m = 0$. In computing the zeros, (16) and (17) are solved numerically by the IMSL subroutine DZEAL, which uses Mueller's method of zero finding. Further discussion on the frequency classification of $P_\ell^m(t)$ can be found in, for example, Haines (1988), Hwang (1991) and Li *et al.* (1995).

2.4 Fully normalized associated Legendre functions of general type

For ease of application, it is necessary to obtain the normalized associated Legendre functions. Let $P_{\ell_i}^m(t)$ and $P_{\ell_j}^m(t)$ be two functions satisfying (11). For $P_{\ell_i}^m(t)$ and $P_{\ell_j}^m(t)$ we multiply one function's differential equation by the other function and take the difference of the two resulting equations. Integrating the final equation over $t_0 \le t \le 1$, we obtain

$$(\ell_j - \ell_i)(\ell_i + \ell_j + 1)\int_{t_0}^{1} P_{\ell_i}^m(t)P_{\ell_j}^m(t)\,dt = (1 - t_0^2)\left[P_{\ell_i}^m(t_0)\frac{dP_{\ell_j}^m(t_0)}{dt} - P_{\ell_j}^m(t_0)\frac{dP_{\ell_i}^m(t_0)}{dt}\right]. \tag{18}$$

By treating ℓ_j as a variable approaching ℓ_i and applying

Table 1. Zeros up to index (n) and order (m) 8 for $\theta_0 = 10°$ ($t_0 = \cos\theta_0$).

(a) $P_\ell^m(t_0) = 0$

n\m	0	1	2	3	4	5	6	7	8
0	13.28								
1	31.13	21.46							
2	49.08	39.70	28.95						
3	67.06	57.79	47.74	36.10					
4	85.05	75.84	66.09	55.45	43.04				
5	103.04	93.87	84.28	74.09	62.94	49.84			
6	121.03	111.89	102.41	92.47	81.88	70.25	56.53		
7	139.03	129.91	120.50	110.72	100.46	89.50	77.44	63.15	
8	157.03	147.92	138.56	128.90	118.85	108.28	96.99	84.52	69.70

(b) $\left.\frac{dP_\ell^m(t)}{dt}\right|_{t=t_0} = 0$

n\m	0	1	2	3	4	5	6	7	8
0	0.00								
1	21.46	10.08							
2	39.70	30.06	17.05						
3	57.79	48.42	37.94	23.65					
4	75.84	66.57	56.63	45.46	30.07				
5	93.87	84.67	74.97	64.53	52.74	36.38			
6	111.89	102.72	93.17	83.09	72.20	59.85	42.63		
7	129.91	120.77	111.31	101.44	91.00	79.69	66.83	48.82	
8	147.92	138.80	129.40	119.68	109.51	98.74	87.05	73.71	54.98

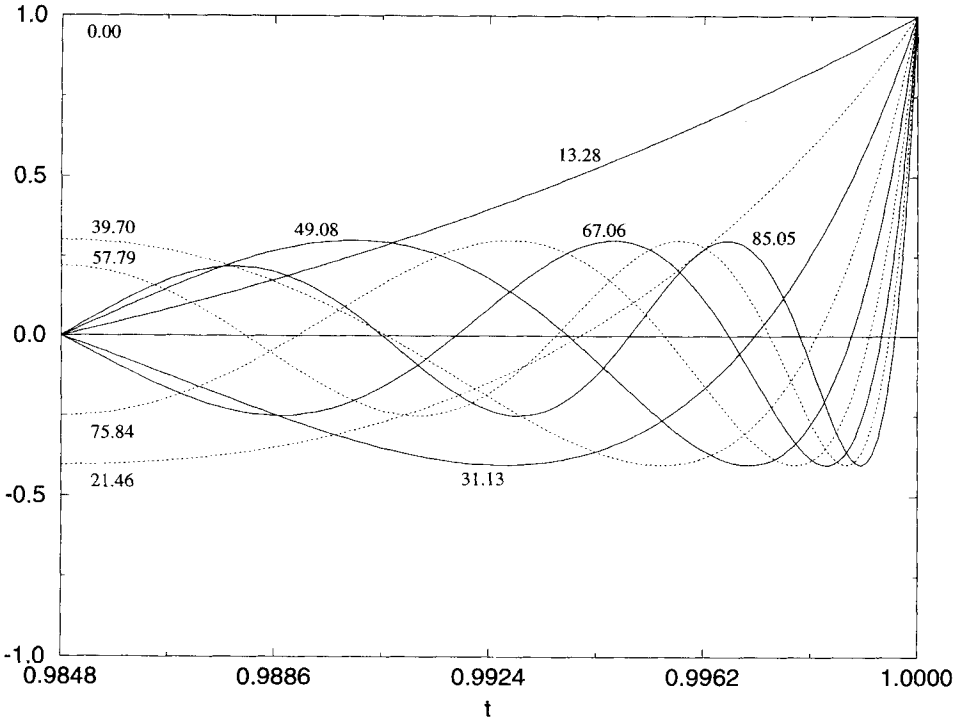

Figure 1. The first five associated Legendre functions of non-integral degree for $\theta_0 = 10°$ and $m = 0$. The solid curves satisfy $P_\ell^m(t_0) = 0$, and the dotted curves satisfy $dP_\ell^m(t)/dt|_{t=t_0} = 0$. The numbers next to the curves are the ℓ values.

L'Hospital's rule, we have

Set 1: $P_{\ell_i}^m(t_0) = 0$, m given

$$I_{\ell_i}^m = \int_{t_0}^1 (P_{\ell_i}^m(t))^2\, dt$$

$$= \lim_{\ell_j \to \ell_i} \frac{(1-t_0^2)\left[P_{\ell_i}^m(t_0)\dfrac{dP_{\ell_j}^m(t_0)}{dt} - P_{\ell_j}^m(t_0)\dfrac{dP_{\ell_i}^m(t_0)}{dt}\right]}{(\ell_j - \ell_i)(\ell_i + \ell_j + 1)}$$

$$= \frac{(t_0^2-1)}{2\ell_i + 1}\frac{\partial}{\partial \ell}[P_{\ell_i}^m(t_0)]\frac{dP_{\ell_i}^m(t_0)}{dt}. \tag{19}$$

Set 2: $\dfrac{dP_{\ell_i}^m(t_0)}{dt} = 0$, m given

$$K_{\ell_i}^m = \int_{t_0}^1 (P_{\ell_i}^m(t))^2\, dt = \frac{(1-t_0^2)}{2\ell_i + 1} P_{\ell_i}^m(t_0)\frac{\partial}{\partial \ell}\left[\frac{dP_{\ell_i}^m(t_0)}{dt}\right]. \tag{20}$$

To complete (19) and (20) we shall derive expressions for

$$\frac{\partial}{\partial \ell}(P_\ell^m(t)) \quad \text{and} \quad \frac{\partial}{\partial \ell}(dP_\ell^m(t)/dt).$$

First, we recall the definition of the ψ-function:

$$\psi(z) = \frac{d\Gamma/dz}{\Gamma(z)} = -\gamma + \sum_{n=0}^{\infty}\left(\frac{1}{n+1} - \frac{1}{n+z}\right), \quad z > 0, \tag{21}$$

where $\gamma = 0.5772156$ is Euler's constant, and the property

$$\psi(z+k) = \psi(z) + \sum_{n=0}^{k-1}\frac{1}{z+n}, \quad k \geq 1 \tag{22}$$

holds. Also, the derivative of the shifted factorial is easily derived as

$$\frac{d}{dz}[(z)_n] = (z)_n \sum_{k=0}^{n-1}\frac{1}{z+k}. \tag{23}$$

Thus we have

$$\frac{\partial}{\partial \ell}(P_\ell^m(t)) = \frac{\Gamma(\ell+m+1)}{2^m m!\Gamma(\ell-m+1)}(1-t^2)^{m/2} \times \sum_{k=0}^{\infty} a_k(b_\ell^m + \beta_k)\left(\frac{1-t}{2}\right)^k$$

$$= \frac{\Gamma(\ell+m+1)}{2^m m!\Gamma(\ell-m+1)}(1-t^2)^{m/2} G(\ell, m, t), \tag{24}$$

and

$$(t^2-1)\frac{\partial}{\partial \ell}\left(\frac{dP_\ell^m(t)}{dt}\right) = tP_\ell^m - P_{\ell-1}^m + \ell t\frac{\partial}{\partial \ell}(P_\ell^m) - (\ell+m)\frac{\partial}{\partial \ell}(P_{\ell-1}^m), \tag{25}$$

where

$$b_\ell^0 = 0, \; b_\ell^m = \sum_{n=0}^{2m-1}\frac{1}{\ell - m + 1 + n}, \quad m > 0, \tag{26}$$

$$\beta_0 = 0, \; \beta_k = -(2\ell+1)\sum_{n=0}^{k-1}\frac{1}{(m+\ell+1+n)(m-\ell+n)}, \quad k > 0. \tag{27}$$

Using the results in (19) and (20), we define two sets of fully

normalized associated Legendre functions of general type:

Set 1

$$\bar{P}_{\ell}^{m}(t) = \sqrt{\frac{[2-\delta(m)](1-t_0)}{I_{\ell}^{m}}}\,P_{\ell}^{m} = \sqrt{\frac{[2-\delta(m)](1-t_0)(2\ell+1)}{G(\ell,m,t_0)H(\ell,m,t_0)}}\left(\frac{1-t^2}{1-t_0^2}\right)^{m/2}F(\ell,m,t). \tag{28}$$

Set 2

$$\bar{P}_{\ell}^{m}(t) = \sqrt{\frac{[2-\delta(m)](1-t_0)}{K_{\ell}^{m}}}\,P_{\ell}^{m} = \sqrt{\frac{[2-\delta(m)](1-t_0)(2\ell+1)}{J(\ell,m,t_0)F(\ell,m,t_0)}}\left(\frac{1-t^2}{1-t_0^2}\right)^{m/2}F(\ell,m,t), \tag{29}$$

where

$$\delta(m) = \begin{Bmatrix} 1, & m=0 \\ 0, & m\neq 0 \end{Bmatrix}, \tag{30}$$

$$H(\ell,m,t_0) = (\ell-m)F(\ell-1,m,t_0) - \ell F(\ell,m,t_0), \tag{31}$$

$$J(\ell,m,t_0) = (\ell-m)G(\ell-1,m,t_0) - \ell t_0 G(\ell,m,t_0) + \frac{\ell-m}{\ell+m}F(\ell-1,m,t_0) - t_0 F(\ell,m,t_0). \tag{32}$$

Here the normalization is 'Heiskanen and Moritz' normalization, which takes into account the area average by introducing the factor $[2-\delta(m)](1-t_0)$, and we have used the term 'fully' by analogy with fully normalized spherical harmonics. Again, the fully normalized associated Legendre functions are represented by the hypergeometric functions. However, unlike the expression in (6), which requires the computation of the sometimes excessively large gamma function, the expressions in (31) and (32) do not contain the gamma function and are numerically manageable for all (ℓ, m) pairs (the values of F, G, H, J will not create overflow or underflow in a computer). In fact, apart from the normalizing factors, the Set 1 and Set 2 functions correspond to Haines' (1985a) 'odd' and 'even' functions, respectively.

2.5 Expansion in series of fully normalized spherical cap harmonics

For an application of the fully normalized associated Legendre functions, we consider the series expansion of an arbitrary function defined over a cap on the spherical earth, whose geometry is shown in Fig. 2. The coordinates of a point on the cap are: θ, the angle between the radial axis through the cap pole and the radial axis through the point, and λ, the angle between the meridian through the north pole and the cap pole and the great circle through the cap pole and the point, measured on the new 'equator' defined by the cap pole. If the function is defined in the geodetic coordinate system, the geodetic coordinates must be first transformed to the cap coordinates (θ, λ). Such a transformation formula can be found in, for example, De Santis, Kerridge & Barraclough (1989). Furthermore, for spherical cap harmonic analyses of vector fields such as deflections of the vertical and the geomagnetic field, the field components in the geodetic coordinate system must be rotated to the components in the cap coordinate system (De Santis *et al.* 1989, p. 10), where one axis is directed to the cap pole and the other directed to a direction 90° clockwise from the cap pole on a local tangential plane.

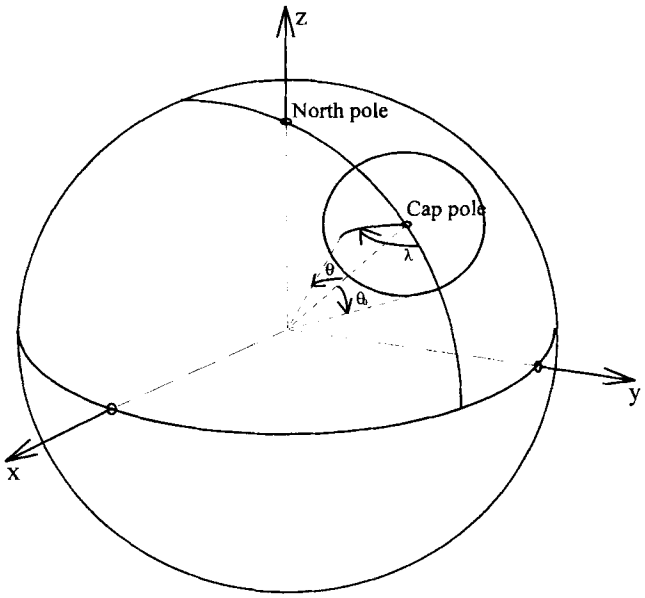

Figure 2. A cap on the earth (approximated by a sphere). The cap size is θ_0 and (θ, λ) are the cap coordinates.

By setting $t = \cos\theta$, the fully normalized associated Legendre functions form a complete set in the variable θ. Also, the classical Fourier functions $\cos m\lambda$ and $\sin m\lambda$ form a complete set in λ. With these two complete sets in variables t and λ we define the fully normalized spherical cap harmonics over a spherical cap:

$$\begin{Bmatrix} \bar{R}_{\ell}^{m}(\theta,\lambda) \\ \bar{S}_{\ell}^{m}(\theta,\lambda) \end{Bmatrix} = \bar{P}_{\ell}^{m}(\cos\theta)\begin{Bmatrix} \cos m\lambda \\ \sin m\lambda \end{Bmatrix}. \tag{33}$$

We shall call the basis functions defined in (33) Set 1 or Set 2 harmonics, depending on which $\bar{P}_{\ell}^{m}$ is used [see (28) and (29)]. Similar to the case for fully normalized spherical harmonics for the unit sphere (Heiskanen & Moritz 1967), the average square of any fully normalized spherical cap harmonic over the spherical cap σ is unity:

$$\frac{1}{2\pi(1-\cos\theta_0)}\iint_{\sigma}(\bar{R}_{\ell}^{m})^2\,d\sigma = \frac{1}{2\pi(1-\cos\theta_0)}\iint_{\sigma}(\bar{S}_{\ell}^{m})^2\,d\sigma = 1. \tag{34}$$

The area of the cap is $2\pi(1-\cos\theta_0)$. These two sets of fully normalized spherical cap harmonics differ from those introduced by Haines (1985a) by the different normalization constant.

A function defined over a spherical cap can be expanded into a series of spherical cap harmonics belonging to Set 1 or Set 2, according to the set chosen for the analysis:

$$f(\theta,\lambda) = \sum_{n=0}^{Nmax}\sum_{m=0}^{n}\left[a_{\ell_n m}\bar{R}_{\ell_n}^{m}(\theta,\lambda) + b_{\ell_n m}\bar{S}_{\ell_n}^{m}(\theta,\lambda)\right], \tag{35}$$

where *Nmax* is the maximum degree of expansion and the

coefficients can be found from

$$\begin{Bmatrix} a_{\ell_n m} \\ b_{\ell_n m} \end{Bmatrix} = \frac{1}{2\pi(1-\cos\theta_0)} \iint_\sigma f(\theta,\lambda) \begin{Bmatrix} \bar{R}^m_{\ell_n}(\theta,\lambda) \\ \bar{S}^m_{\ell_n}(\theta,\lambda) \end{Bmatrix} d\sigma. \qquad (36)$$

Note that this equation is valid for one-set analysis and does not apply when both sets are used simultaneously. If $f(\theta, \lambda)$ is not known everywhere over the spherical cap, the coefficients can be found by the least-squares method. The spatial resolution corresponding to the expansion in (35) over a cap of spherical earth is $R\theta_0/Nmax$, where R is the mean earth radius (Li *et al.* 1995).

Using the frequency classification of $\bar{P}^m_{\ell_n}(\cos\theta)$ as stated before and the fact that the functions $\cos m\lambda$ and $\sin m\lambda$ have $2m$ zeros over $0 \le \lambda < 2\pi$, the harmonics defined in (33) with degree ℓ_n for the cases $m = 0$, $n > m$, and $n = m$ may be termed zonal, tesseral and sectorial spherical cap harmonics, respectively, similar to the geometrical representation of spherical harmonics on the unit sphere. Furthermore, the average power of $f(\theta, \lambda)$ at index n is

$$\tau_n^2 = \frac{1}{2\pi(1-\cos\theta_0)} \times \iint_\sigma \left\{ \sum_{m=0}^{n} (a_{\ell_n m}\cos m\lambda + b_{\ell_n m}\sin m\lambda)\bar{P}^m_{\ell_n}(\cos\theta) \right\}^2 d\sigma = \sum_{m=0}^{n} (a^2_{\ell_n m} + b^2_{\ell_n m}), \qquad (37)$$

which can also be called the degree variance at index n, similar to the degree variance of a spherical harmonic expansion. τ_n^2 is a measure of energy at index n; see also the discussion by Haines (1991). Note that the normalization for the associated Legendre functions must be exact in order to obtain τ_n^2 using (37).

In this study we propose the use of just one set of cap harmonics (Set 1 or Set 2) in an expansion, in contrast to the approach of Haines (1985a) who used both sets simultaneously. The convergent rate of an expansion with two sets may be faster than that of an expansion with just one set, because in the former case any boundary condition is satisfied. However, since the functions in Set 1 are not orthogonal to the functions in Set 2, the 'spectral' components from a two-set expansion will be mutually dependent (Hwang 1991). Furthermore, orthogonal functions arising from the eigenvalue–eigenfunction problem form a complete set of functions, and the use of a complete set of functions will guarantee that the expansion of an arbitrary function (not necessarily satisfying any boundary conditions) is convergent in the mean (Tolstov 1976). Convergence in the mean is less stringent than uniform convergence (Davis 1975), and it tolerates bad fits between the expanded function and the expansion at a finite number of points. See also the discussion by Haines (1990) and the numerical examples below.

3 APPLICATIONS TO THE ANALYSIS OF SEA-LEVEL DATA FROM TOPEX/POSEIDON AND ERS-1

3.1 The sea-level data

The basic sea-level data type for our analysis is the sea-surface topography (SST), which is the difference between the sea surface and the marine geoid. Sea-level anomaly (SLA) is the difference between the SST defined at given epoch or over a short period of time and the mean SST. In this work, the sea-level data were derived from TOPEX/POSEIDON (T/P) and ERS-1 altimetry. We obtained the 10-day T/P SST from cycle 2 to 117 from the Center for Space Research (CSR), University of Texas, Austin, who have computed the T/P orbits with the latest gravity model JGM3 of the Joint Gravity Model series (Nerem *et al.* 1994). The CSR used the CSR 3.0 tide model for the tidal corrections and a hybrid geoid (coefficients of JGM3 from degree 2 to 70, and coefficients of OSU91A from degree 71 to 360) in the SST derivation. Also, a three-year averaged SST is available from CSR for deriving SLA. For ERS-1 we used the corrected sea-surface heights (SSH) from Le Traon *et al.* (1995), who have adjusted the ERS-1 orbits to make ERS-1's orbital accuracy compatible with T/P's. Because of the use of concurrent orbits in the adjustment, the ERS-1 35-day repeat SSH cover only cycles 6 to 18. We computed the same hybrid geoid as used in the T/P SST on a $30' \times 30'$ grid and then interpolated the geoidal heights to the ERS-1 data points to get ERS-1's SST.

3.2 Expansion of sea-level anomaly

First we shall test various aspects of the performance of Set 1 and Set 2 harmonics [see (33)]. We expand the SLA from cycle 2 of T/P for the western Pacific using Set 1 and 2 harmonics separately up to $Nmax = 6$ by the least-squares method. The cap pole is at 7°S, 160°E, and the cap size is $\theta_0 = 10°$. Fig. 3 shows the results. From Fig. 3, we see that the two expansions look quite similar, but large differences exist at the cap boundary. While discontinuity exists at the boundary in the expansion using Set 1 harmonics, the expansion using Set 2 functions transits smoothly from the interior to the border. This is due to the fact that an arbitrary function such as SLA will not necessarily satisfy the boundary condition $P^m_\ell(t_0) = 0$ or $dP^m_\ell(t)/dt|_{t=t_0} = 0$, but the value of the function can be easily adjusted to satisfy $dP^m_\ell(t)/dt|_{t=t_0} = 0$, so the latter condition results in a smooth transition at the boundary.

Fig. 4 shows the root-mean-squared (rms) differences between the original data and the expansions, which suggests that for the same expansion degree the use of Set 2 harmonics results in a faster convergence than the use of Set 1 harmonics. An advantage of cap harmonic expansion with just one set is its ability to spectrally decompose a local signal on the sphere without the problems of aliasing and singularity that occur in the expansion using global functions such as spherical harmonics (Hwang 1993). Fig. 5 shows the degree variances of SLA from the two expansions. For both expansions the zero degrees contain most of the energy, and the degree variance decays rapidly as the index increases.

The conclusion of this example is that the two expansions give almost identical results, but to have a faster convergence and to avoid discontinuity at the cap boundary it is advisable to use Set 2 harmonics, unless the expanded function satisfies Dirichlet's boundary condition. The faster convergence of Set 2 harmonics agrees with Haines' (1990) result. The simultaneous use of Set 1 and Set 2 may provide a better fit of the data at the expense of the ability to make a spectral decomposition of the signal under study. This can be particularly advantageous when the spherical cap harmonic expansion is actually 3-D [i.e., there is also a radial term on both sides of (35)] and the

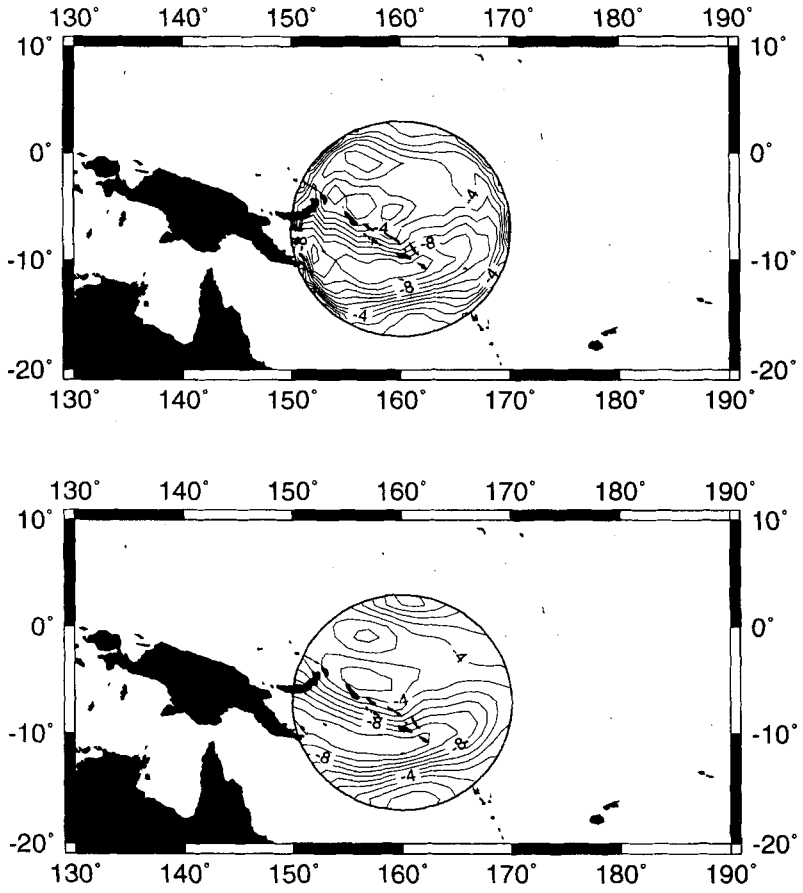

Figure 3. Spherical cap harmonic expansions of sea-level anomaly from cycle 2 of T/P up to $n = m = 6$ for the western Pacific using Set 1 harmonics (top) and Set 2 harmonics (bottom). Contour interval is 1 cm.

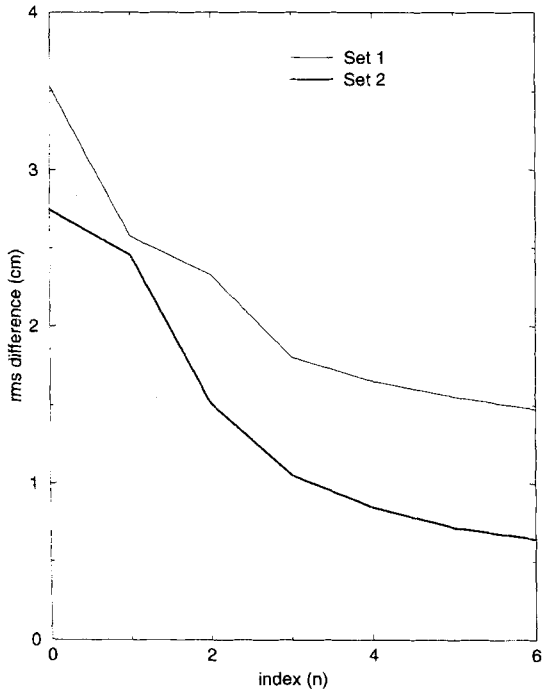

Figure 4. Root-mean-squared differences between the original sea-level anomalies and the spherical cap harmonic expansions up to $Nmax = 6$ (see Fig. 3).

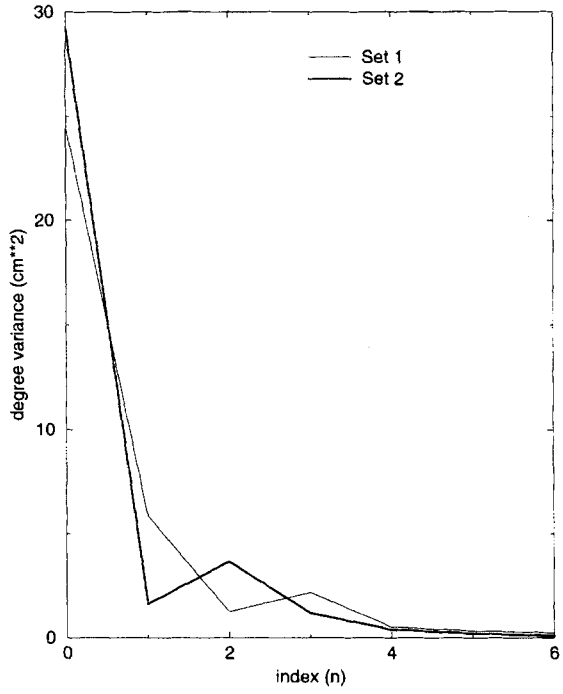

Figure 5. Degree variances of sea-level anomaly from the spherical cap harmonic expansions up to $Nmax = 6$ (see Fig. 3).

data are the components of the gradient of a Laplacian potential as in geomagnetic field analysis (e.g. Haines 1985a; De Santis *et al.* 1989), since possible boundary misfits, which are more significant with one-set analysis because of their unphysical boundary conditions, have serious consequences even inside the region. Note that the SLA of T/P from CSR have been smoothed according to the CSR's data documentations. For such SLA we have found that the variation of the cap harmonic coefficients from using different *Nmax* [see (35)] is small.

3.3 Zero-degree coefficient of sea-level anomaly as a Southern Oscillation Index

The next application is for the study of El Niño. El Niño is caused in part by a large downwelling Kelvin wave travelling eastwards across the equatorial Pacific Ocean (Apel 1987). There are several definitions associated with El Niño. A recent definition is that 'El Niño is underway when sea level at Galapagos is 2 cm above its normal height for six or more consecutive months' (Meyers & O'Brien 1995). To test the ability of T/P and ERS-1 in detecting El Niño, we computed the zero-degree coefficients $a_{\ell_0 0}$ of SLA from cycle 2 to 117 of T/P and cycle 6 to 18 of ERS-1 using Set 2 harmonics for the eastern Pacific. The cap pole is near Galapagos and is at 1°S, 268°E, and the cap size is 10°. We also computed $a_{\ell_0 0}$ of SLA for the western Pacific (the same area as shown in Fig. 3). From the definition of Set 2 harmonics, we see that the geometrical meaning of $a_{\ell_0 0}$ is the area-average of the expanded function over the spherical cap. Figs 6 and 7 show the values $a_{\ell_0 0}$ for the western and eastern Pacific from the SLA of T/P and ERS-1, respectively. Except for cycles 16, 17 and 20, T/P's zero-degree coefficients from cycle 13 to 30 all exceed 2 cm. The period corresponding to cycle 13 to 30 is between 1993 January and 1993 July, lasting for 7 months. Thus, according to the new definition of El Niño, T/P's zero-degree coefficients have signified the occurrence of El Niño during the 1993 January–1993 July period. Indeed, other data have shown that El Niño occurred during that period (Meyers & O'Brien 1995; Boulanger & Menkes 1995). ERS-1's zero-degree coefficients from cycle 8 to 14 also show a similar trend in SLA during that El Niño event, but only the coefficients from cycles 11, 12

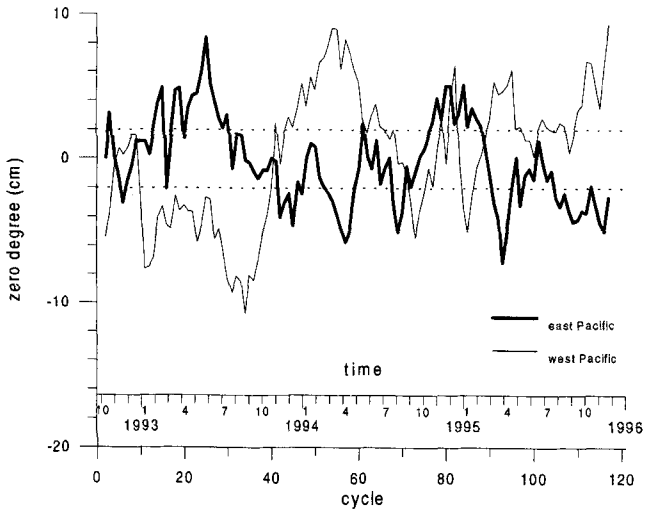

Figure 6. Time series of zero-degree coefficients $a_{\ell_0 0}$ of sea-level anomaly from cycle 2 to 117 of T/P for the western and eastern Pacific.

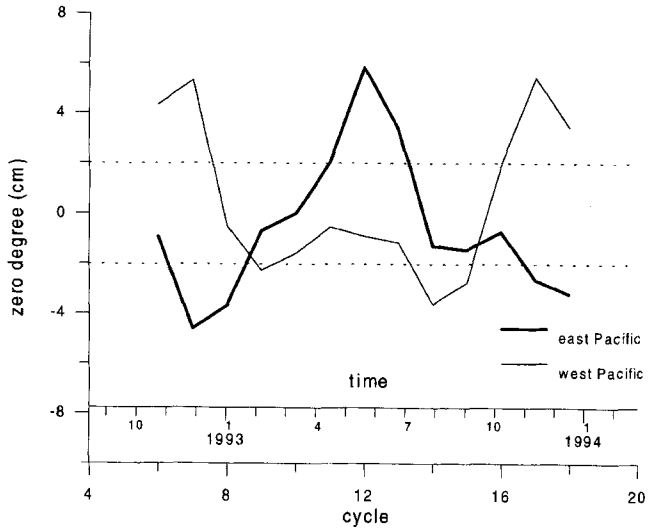

Figure 7. Time series of zero-degree coefficients $a_{\ell_0 0}$ of sea-level anomaly from cycle 6 to 18 of ERS-1 for the western and eastern Pacific.

and 13 (total 3.5 months) exceed 2 cm. Furthermore, T/P's zero-degree coefficients of SLA for the western Pacific from cycle 43 to 68 (1993 November to 1994 July) are all larger than 2 cm—this may indicate the occurrence of La Niña, the cold event of El Niño (Philander 1990). Although the ERS-1 data record is not long enough to account for the whole La Niña event, ERS-1's zero-degree coefficient for the western Pacific also starts to increase from cycle 16 (near cycle 43 of T/P in time), implying the initiation of La Niña. From Fig. 6, we see that, during the 1992–1993 El Niño, the lowest anomaly in the western Pacific occurred at cycle 11, while the largest anomaly in the eastern Pacific occurred at cycle 25, so the two peaks have a time gap of 4–5 months, and this may give a hint to the propagating time of the Kelvin wave. In conclusion, the zero-degree coefficient can be of use to the study of El Niño, or even can serve as a Southern Oscillation Index.

3.4 Western boundary currents and basin-scale circulations

The study of the global circulation is one of the main objectives of many altimeter missions such as T/P, but in many cases one wishes to analyse local circulation systems, which may require the use of local basis functions such as the cap harmonics. Furthermore, unless a high-resolution and high-accuracy geoid model is available, altimeter data can only identify low-frequency features of the ocean's circulations (Tapley *et al.* 1994). In the present example, we shall examine the performance of the cap harmonic expansions in identifying local features that are related to the western boundary currents and basin-scale circulations. Fig. 8 shows the expansion of the yearly averaged ERS-1 SST over the Kuroshio area up to $Nmax = 3$ using Set 2 harmonics (the reason for using averaged SST is due to the large data gaps resulting from bad wet tropospheric corrections at this area). The cap pole is at 18°N, 138°E, and the cap size is 18°. With only 16 coefficients the expansion clearly identifies the feature associated with the Kuroshio Current. To see basin-scale circulations, we expand the SST from cycle 47 of T/P over the South China Sea using Set 2 harmonics up to $Nmax = 6$. The result is shown in Fig. 9.

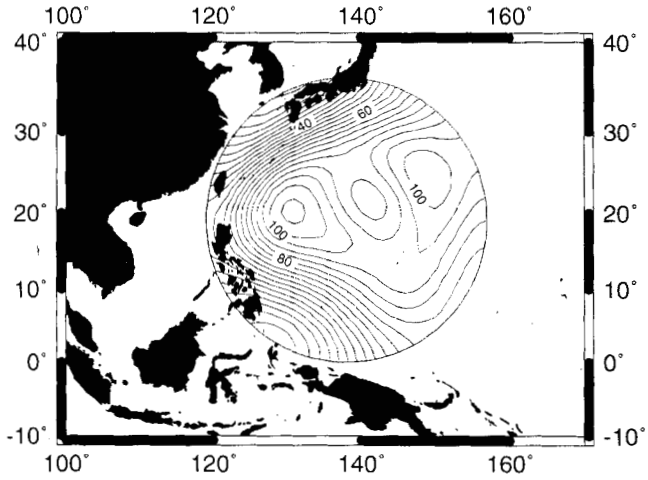

Figure 8. Spherical cap harmonic expansion of yearly averaged sea-surface topography from ERS-I up to $Nmax = 3$ for the Kuroshio area. Contour interval is 5 cm.

The cap pole is at 14°N, 115°E, and the cap size is 10°. Because of the geostrophic balance, the streamlines in Fig. 9 suggest that the circulation over the South China Sea is cyclonic, which is consistent with the result implied by surface drifters; see, for example Soong *et al.* (1995). Soong *et al.* (1995) also discovered a cold-core eddy in the northern part of the South China Sea during the cycle 47 period. This cold-core eddy is clearly visible in Fig. 9. These two examples show that the cap harmonic expansions can work properly as a filter to extract large-scale oceanographic signals in the presence of geoidal error.

3.5 The average kinetic energy of an eddy

In Fig. 9 we have identified a cold-core eddy over the South China Sea and now we wish to study its kinetic energy. To this end, we shall use a property of eigenfunctions: the eigenvalue of an eigenfunction is equal to the integrated squared gradients of the eigenfunction over the fundamental domain. On a sphere of radius R, this property is expressed as (Morse & Feshbach 1953; Hwang 1991)

$$\kappa = \iint_{\sigma} (\nabla u \cdot \nabla u)\, d\sigma, \tag{38}$$

where κ is the eigenvalue of u, ∇ is the gradient operator

$$\nabla = \left(\frac{\partial}{R \sin\theta \partial\lambda} \frac{\partial}{R\partial\theta} \right), \tag{39}$$

and u must be orthonormalized so that the scalar product of u with u is unity. Now, the geostrophic velocity components of an eddy along the longitudinal and the poleward directions are (Apel 1987)

$$\begin{Bmatrix} v_\lambda \\ v_\theta \end{Bmatrix} = \frac{g}{f} \begin{Bmatrix} \dfrac{\partial\zeta}{R\partial\theta} \\ \dfrac{\partial\zeta}{R \sin\theta \partial\lambda} \end{Bmatrix}, \tag{40}$$

where ζ is the SST, g is the earth's normal gravity, and $f = 2\omega \sin\phi$ with ω being the earth's rotational velocity and ϕ the geodetic latitude. Although the velocity components in (40) are expressed in the cap coordinate system, the quantity $\nabla u \cdot \nabla u$ is invariant under coordinate transformation. Thus, assuming that g and f in (40) are constants and an eddy can

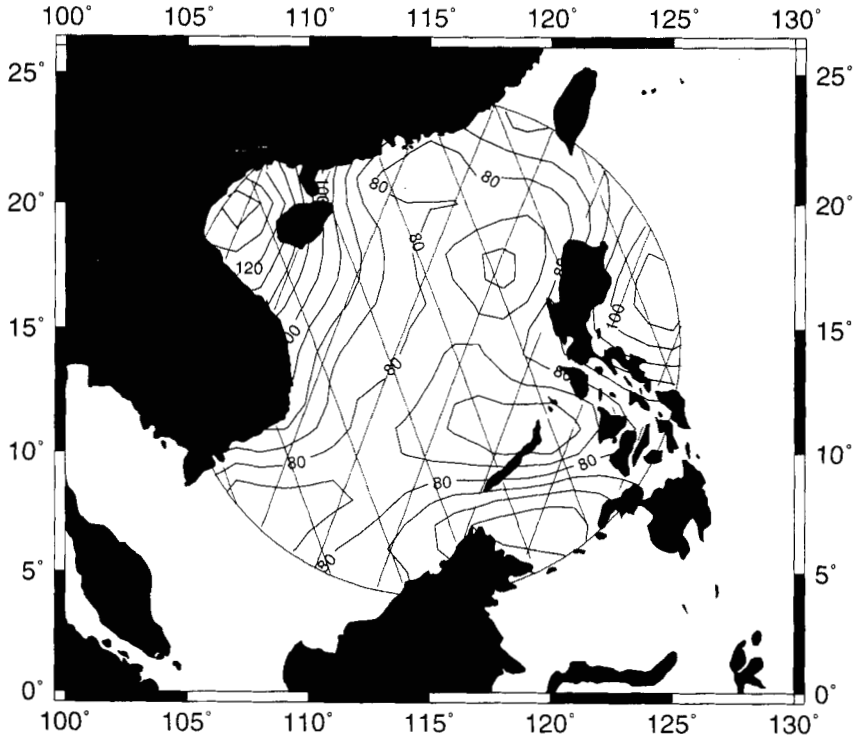

Figure 9. Spherical cap harmonic expansion of sea-surface topography from cycle 47 of T/P up to $Mmax = 6$ over the South China Sea. Also plotted are the ground tracks of T/P. Contour interval is 5 cm. A cold-core eddy centred at 17.5°N, 118°E and with a radius of 2° is clearly visible.

be represented by a cap harmonic, the averaged kinetic energy per unit mass of the eddy is

$$KE = \frac{1}{2\pi(1-\cos\theta_0)} \int\int_\sigma \frac{1}{2} V^2 \, d\sigma = \frac{1}{2} \frac{g^2 c_{\ell m}^2}{f^2 R^2} \ell(\ell+1), \qquad (41)$$

where $R \approx 6371$ km and $c_{\ell m}$ is the coefficient of the cap harmonic. Considering an eddy as a vibrating membrane with radial symmetry [see also Gründlingh (1995, Fig. 4) for the support of this statement] the zonal cap harmonics ($m = 0$) will best approximate its shape if the core of the eddy is situated at the cap centre. However, the sense of the rotation of an eddy is uniform within the eddy field, so only $\bar{P}^0_{\ell_0}(t)$ of Set 1 and $\bar{P}^0_{\ell_1}(t)$ of Set 2 will satisfy this condition because their gradients do not change sign over the cap (see Fig. 1).

As an example, we approximated the SST from cycle 29 to 65 (a total of one year) of T/P over the cold-core eddy found in Fig. 9 by $\bar{P}^0_{\ell_0}(t)$ of Set 1. The cap pole is at 17.5°N, 118°E, and the cap size is 2°. With the coefficients found, we computed the kinetic energy using (50). Fig. 10 shows the relative kinetic energy of the eddy with respect to the yearly mean kinetic energy. Fig. 10 indicates that the cold-core eddy has almost the lowest kinetic energy during the cycle 47 period (winter), and it has the highest kinetic energy in the summer. The variation of the eddy's kinetic energy during that particular year seems to be periodic with an amplitude of 0.4 $m^2 s^{-2}$, and this phenomenon should be closely linked to the seasonal cycle of ocean dynamics. Note that in this analysis we have assumed that the centre and the dimension of the eddy did not change during that year, which is quite reasonable as we have investigated the eddy geometry from other T/P cycles.

4 CONCLUSION

In this paper we introduce two sets of fully normalized spherical cap harmonics, which are the equivalents of the fully normalized spherical harmonics of Heiskanen & Moritz (1967) on a spherical cap. We also present formulae for finding the zeros without numerical problems, and formulae for computing the fully normalized associated Legendre functions of non-integer degree without using the gamma function or the shifted factorial. We successfully use the cap harmonic expansions to do analyses of sea-level data from T/P and ERS-1 for problems ranging from the spectral analysis of SLA to the computation of eddy kinetic energy and its evolution. In terms of approximating a function on a spherical cap, the use of a cap harmonic expansion is very economical and stable, because only relatively few terms are needed and there is no aliasing or numerical singularity. More applications of cap harmonic expansion, such as comparing the SST spectra and the error spectra of a geoid model for the determination of SST cut-off frequency (Tapley *et al.* 1994), can be expected.

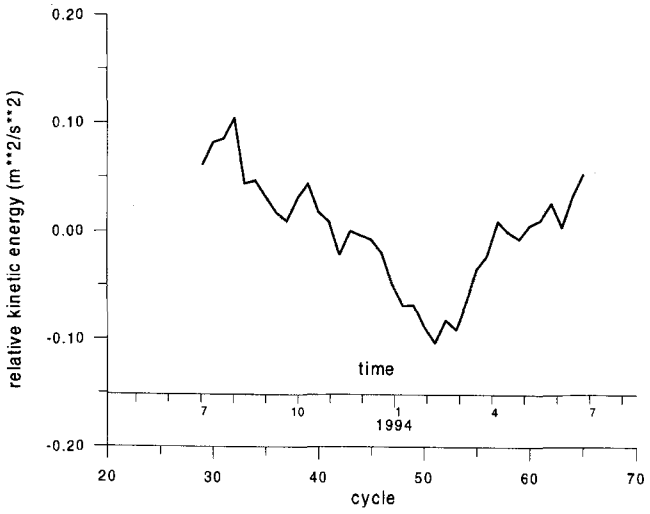

Figure 10. Relative average kinetic energy of the cold-core eddy over the northern South China Sea (see Fig. 9) from cycle 29 to 65 of T/P.

ACKNOWLEDGMENTS

This study is supported by the National Science Council of ROC, under contract NSC-85-2211-E-009-019. We thank CSR of UT, Austin, for the convenient access of the most up-to-date TOPEX/POSEIDON data via the Internet. We thank AVISO for sending us the corrected ERS-1 altimetry, and Angelo De Santis and an anonymous reviewer for their constructive suggestions that improved the quality of the paper. Figs 3, 8 and 9 were made with GMT (Wessel & Smith 1995).

REFERENCES

Apel, J.R., 1987. *Principles of Ocean Physics,* Academic Press, New York, NY.

Boulanger, J.P. & Menkes, C., 1995. Propagation and reflection of long equatorial waves in the Pacific Ocean during the 1992–1993 El Niño, *J. geophys. Res.,* **100,** 25 041–25 059.

Courant, R. & Hilbert, D., 1953. *Methods of Mathematical Physics,* Vol. I, Interscience, New York, NY.

Davis, P.J., 1975. *Interpolation and Approximation,* Dover, New York, NY.

De Santis, A., 1991. Translated origin spherical cap harmonics analysis, *Geophy. J. Int.,* **106,** 253–263.

De Santis, A., 1992. A conventional spherical harmonic analysis for region modeling of the geomagnetic field, *Geophy. Res. Lett.,* **19,** 1065–1067.

De Santis, A. & Falcone, C., 1995. Spherical cap models of Laplacian potentials and general fields, in *Geodetic Theory Today,* pp. 141–150, ed. Sansó, F., Springer, New York.

De Santis, A., Kerridge, D.J. & Barraclough, D.R., 1989. A spherical cap harmonic model of the crustal magnetic anomaly field in Europe observed by Magsat, in *Geomagnetism and Palaeomagnetism,* eds Lowes, F.J. *et al.,* Nato ASI Series, Vol. 261, pp. 1–17.

Gründlingh, M.L., 1995. Tracking eddies in the southeast Atlantic and southwest Indian oceans with TOPEX/POSEIDON, *J. geophys. Res.,* **100,** 24 977–24 986.

Haines, G.V., 1985a. Spherical cap harmonic analysis, *J. geophys. Res.,* **90,** 2583–2591.

Haines, G.V., 1985b. Magsat vertical field anomalies above 40°N from spherical cap harmonic analysis, *J. geophys. Res.,* **90,** 2593–2598.

Haines, G.V., 1988. Computer programs for spherical cap harmonic analysis of potential and general fields, *Computers and Geosciences,* **14,** 413–447.

Haines, G.V., 1990. Modeling by series expansions: a discussion, *J. Geomag. Geoelectr.,* **42,** 1037–1049.

Haines, G.V., 1991. Power spectra of sub-periodic functions, *Physics Earth planet. Inter.,* **65,** 231–247.

Haines, G.V. & Torta, J.M., 1994. Determination of equivalent current sources from spherical cap harmonic models of geomagnetic field variations, *Geophys. J. Int.,* **118,** 499–514.

Heiskanen, W.A. & Moritz, H., 1967. *Physical Geodesy,* W.H. Freeman, New York, NY.

Hobson, E.W., 1965. *The Theory of Spherical and Ellipsoidal Harmoncis,* Second Reprint, Chelsea Publishing Co., New York, NY.

Hwang, C., 1991. Orthogonal functions over the oceans and applications to the determination of orbit, geoid and sea surface topography from satellite altimetry, *Rep. No. 404, Dept. of Geod. Sci. and Surv.,* The Ohio State University, OH.

Hwang, C., 1993. Spectral analysis using orthonormal functions with a case study on the sea surface topography, *Geophys. J. Int.,* **115,** 1148–1160.

Lebedev, N.N., 1972. *Special Functions and Their Applications,* Dover, New York, NY.

Le Traon, P.Y., Caspar, P., Bouyssel, F. & Makhmara, H., 1995. Using TOPEX/POSEIDON data to enhance ERS-1 orbit, *J. Atm. Ocean. Tech.,* **12,** 161–170.

Li, J., Chao, D. & Ning, J., 1995. Spherical cap harmonic expansion for local gravity field representation, *Manuscripta geodaetica,* **20,** 265–277.

Meyers, S.D. & O'Brien, J.J., 1995. Pacific Ocean influences atmospheric Carbon Dioxide, *EOS, Trans. Am. geophys. Un.,* **76,** 533–537.

Morse, P.M. & Feshbach, H., 1953. *Methods of Theoretical Physics,* McGraw-Hill, New York, NY.

Nerem, R.S. *et al.,* 1994. Gravity model development for TOPEX/POSEIDON: Joint Gravity Models 1 and 2, *J. geophys. Res.,* **99,** 24 421–24 448.

Philander, S.G., 1990. *El Niño, La Niña, and the Southern Oscillation,* Academic Press, New York, NY.

Soong, Y.S., Hu, J.-H., Ho, C.-R. & Niiler, P.P., 1995. Cold-core eddy detected in South China Sea, *EOS, Trans. Am. geophys. Un.,* **76,** 345–347.

Tapley, B.D., Chambers, D.P., Shum, C.K., Eanes, R.J., Ries, J.C. & Stewart, R.H., 1994. Accuracy assessment of the large-scale dynamic ocean topography from TOPEX/POSEIDON altimetry, *J. geophys. Res.,* **99,** 24 605–24 618.

Tolstov, G.P., 1976. *Fourier Series,* trans. by R.A. Silverman, Dover, New York, NY.

Wessel, P. & Smith, W.H.F., 1995. New version of Generic Mapping Tools released, *EOS, Trans. Am. geophys. Un.,* **76,** pp. 329.